ACS OMEGA

http://pubs.acs.org/journal/acsodf

Article

Solid-State Au Nanocone Arrays Substrate for Reliable SERS Profiling of Serum for Disease Diagnosis

Yanyan Lu, Biao Lei, Qian Zhao,* Xiaowei Yang, Yi Wei, Tingting Xiao, Shuyi Zhu, Yu Ouyang,* Hongwen Zhang,* and Weiping Cai

Cite This: *ACS Omega* 2023, 8, 29836−29846

Read Online

ACCESS | Metrics & More | Article Recommendations

ABSTRACT: Surface-enhanced Raman scattering (SERS) is a widely used rapid and noninvasive method for detecting biological substances in serum samples and is commonly employed in disease screening and diagnosis. Solid-state nanoarray SERS substrates used in serum detection may cause spectral instability due to imperfections in the detection method. For the purpose of identifying optimal detection conditions, various dilution levels of the serum were tested in this study. The study found that a complete and stable serum SERS spectrum can be obtained when the serum is diluted by a factor of 50. The study reports the successful preparation of an Au nanocone array (Au NCA) plasmonic substrate with a uniform, controllable microstructure and high activity, achieved through a combination of PS colloidal sphere template-assisted reactive ion etching (RIE) process and magnetron sputtering deposition technology. Based on this substrate, a standard detection scheme was developed to obtain highly stable and repeatable serum SERS spectra. The study verified the reliability of the optimized serum detection scheme by comparing the SERS spectra of serum samples from healthy individuals and gastric cancer patients, and confirmed the potential benefits of the scheme for disease screening and diagnosis.

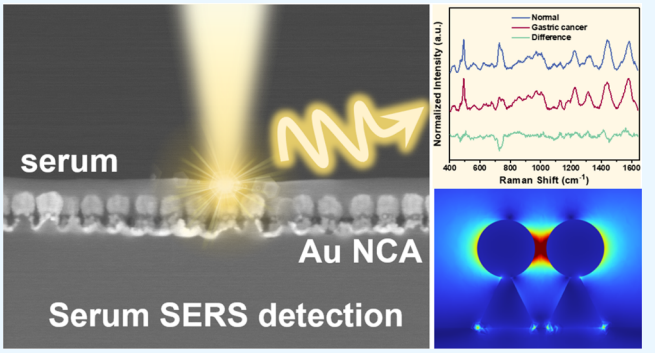

1. INTRODUCTION

In recent years, surface-enhanced Raman spectroscopy (SERS) has gained widespread usage for the detection and identification of molecules through amplifying the characteristic Raman spectra of surface-adsorbed molecules with high enhancement factors (up to 10^8 or more) via the excitation of localized surface plasmon resonances (LSPR) on noble-metal surfaces.[1] This technology has been deployed in numerous areas, including catalysis,[2,3] electrochemistry,[4,5] biology,[6,7] medicine,[8,9] materials science,[10,11] and other applications. Raman spectroscopy, particularly, has been used as a rapid and noninvasive detection tool for disease diagnosis in medical testing.[12] As one of the most sensitive analytical techniques currently available, the SERS technology has proved very useful for a broad range of analytical issues related to biomedical applications.[1] It is well established that almost all diseases, such as tumors, diabetes, and liver damage, are initially caused by molecular-level abnormalities (DNA, RNA, proteins, metabolites, and other biomolecules), which usually lead to changes in the composition and concentration of serum components.[13,14] For instance, α-fetoprotein (AFP) is a widely recognized serum screening marker for hepatocellular carcinoma (HCC). In nonpregnant adults, healthy AFP levels are usually below 10 ng/mL, but they rise significantly when liver cells undergo cancerous changes.[15] Thus, analyzing serum components and concentrations can be an effective way of reflecting physiological and pathological changes in cells and tissues, and plays a crucial role in clinical diagnosis. Raman spectroscopy can indicate precise changes in serum components and concentrations by providing rich and accurate vibrational spectrum information (characteristic peak positions, spectral widths, and intensities), thereby providing the basis for disease diagnosis.[16,17] However, the Raman scattering signal changes are generally small and, due to fluorescence interference, result in a poor signal-to-noise ratio of the spectral signal, making it difficult to identify spectral disparities. SERS, on the other hand, has stronger Raman signals and more precise spectral widths, significantly enhancing the signal-to-noise ratio and making serum sensitivity measurement based on Raman scattering a reality.[18] Furthermore, compared to traditional serum detection

Received: July 9, 2023
Accepted: July 25, 2023
Published: August 3, 2023

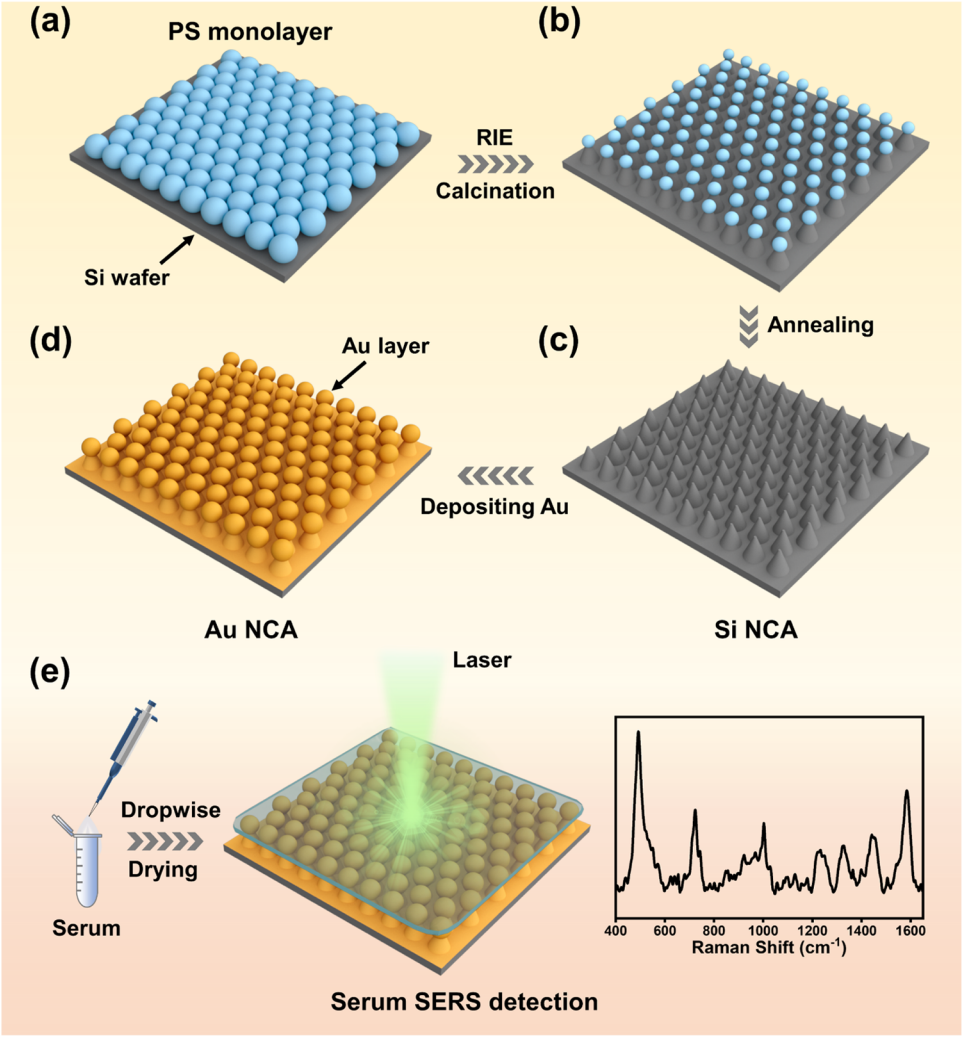

Figure 1. Schematic illustration for the fabrication of Au NCA plasmonic substrate and SERS detection of serum. (a) Self-assembled PS colloidal sphere monolayer template on Si wafer. (b) After etching the template with a mixture of SF_6, Ar, and CHF_3, the etched PS spheres remain on the Si NCA. (c) Si NCA after removal of residual PS spheres by annealing. (d) Au NCA obtained after sputtering deposition. (e) Facile SERS detection of serum.

methods (Immunofluorescence,[19] Enzyme-linked immunosorbent assay (ELISA)[20] and Radioimmunoassay (RIA)[21]), the SERS technology has the benefits of high sensitivity, high selectivity, quantification, high efficiency, and diversity. In recent years, the SERS technology has made significant progress in the field of serum detection, specifically through the synthesis and construction of colloidal Au/Ag enhancement reagents, driven primarily by the technology's advantages.[22,23] For example, Muhammad et al. developed a label-free, highly sensitive, and highly selective biosensor for detecting interleukin-6 (IL-6) in mouse serum using Au nanoparticles (NPs), enabling investigations of drug and bacterial infections.[24] Additionally, to improve the noninvasive cancer detection technology based on serum detection, Jing Wang et al. developed a label-free SERS detection method based on serum protein spectra fingerprint that is capable of clinical detection of colorectal cancer.[25] In summary, the SERS technology is widely used in the field of biomedical research, especially in the detection of serum samples.

Aqueous dispersions of Au NPs and Ag NPs, commonly known as metal colloids, are often utilized SERS substrates for serum detection.[14,26−28] However, residual chemicals during the synthesis process can interfere with serum SERS spectra, complicating clinical serum detection.[29] The long-term storage of metal colloids often leads to the aggregation of metal particles, which can lead to extremely uneven SERS hotspot density, rendering stable serum SERS spectrum acquisition unfavorable.[30,31] As a result, solid-state nanoarray substrates, which are known to have stronger, cleaner, and more stable SERS signals compared to metal colloids, hold promise for serum detection.[10,32] For instance, Yong Wei et al. were able to accurately identify serum samples from both gastric cancer patients and healthy individuals using Au/Ag nanowire arrays prepared via noble-metal-assisted chemical etching reduction.[33] Furthermore, Muhammad and colleagues fabricated Au NPs solid-state substrates by sputtering plasma onto the nanotips of aluminum oxide (AAO) templates, which were employed for the precise detection of serum samples from mice treated with X-ray total body irradiation (TBI), confirming that changes in myoglobin content were due to radiation-induced damage.[34] However, the solid-state substrate has certain shortcomings in that the uniformity and standardization of the serum SERS spectrum cannot be ensured, which is caused by the imperfect serum detection method.[33,35]

https://doi.org/10.1021/acsomega.3c04910
ACS Omega 2023, 8, 29836−29846

As a result, the development of a standardized detection method for obtaining highly stable and reproducible serum SERS spectra using solid-state nanoarray substrates is crucial for the clinical application of serum.

In this study, an Au nanocone array (Au NCA) plasmonic substrate with high activity and uniform and controllable microstructure was developed successfully by combining PS colloidal sphere template-assisted reactive ion etching (RIE) technology and magnetron sputtering deposition technology. Using this substrate, we optimized the standard detection method to obtain serum SERS spectra with high stability and repeatability. Normal human serum was utilized as the research target, and the instability of serum SERS spectra was analyzed. We evaluated the effect of serum thickness and viscosity on serum SERS spectra by varying the serum dilution ratio. The experimental outcomes indicated that serum SERS spectra were complete and highly stable when the serum dilution ratio reached 50 times. Additionally, the optimized serum detection method was deployed in diagnosing gastric cancer. Through the comparative analysis of the characteristic peaks of serum SERS spectra of normal individuals and gastric cancer patients, the reliability of the optimized serum detection method was further verified. This study presents the prerequisites for researching and evaluating reliable SERS-based diagnostic technology. Furthermore, it is expected to provide more accurate and reliable detection methods for clinical medical diagnosis.

2. EXPERIMENTAL SECTION

2.1. Materials and Reagents. Ethanol, acetone, sodium dodecyl sulfate (SDS), and Rhodamine 6G (R6G) were acquired from Sinopharm Chemical Reagent Co., Ltd., in Shanghai, China. The etching gases trifluoromethane (CHF_3), sulfur hexafluoride (SF_6), and argon (Ar) were obtained from Nanjing Special Gas Works Co., Ltd. Suspensions of polystyrene (PS) colloidal spheres, which were 120, 250, and 500 nm in diameter, and 2.5 wt % dispersion in water, along with Si (100) wafers, were procured from Huge Biotechnology in Shanghai, China, and Zhejiang Lijing Silicon Material Co., Ltd., respectively. Au target with 99.999% purity was obtained from ZhongNuo Advanced Material (Beijing) Technology Co., Ltd. Deionized water, with a resistivity of 18.2 MΩ cm, was obtained from an ultrafilter system (Millipore Milli-Q system, Marlborough, MA).

2.2. Collection and Preparation of Clinical Serum Samples. The following protocol was employed for serum sample preparation. Serum samples of 30 healthy volunteers, 30 patients with gastric cancer, and 20 patients with intestinal cancer were kindly collected from the College of Clinical Medicine of Yangzhou University with the same ethnic background, and the College has obtained all participants' informed consent. Sterile conditions were enforced during serum sample collection. After the individuals had fasted for a period of 12 h, 3 mL of peripheral venous blood was collected without the use of anticoagulants. The blood was allowed to stand at room temperature for 2 h before centrifugation at 3500 r/min for 15 min. The resulting supernatant was taken to obtain serum samples, which were subsequently stored at −80 °C in a refrigerated environment until used for SERS spectral measurements during the experimental procedure.

2.3. Fabrication of Au NCA Plasmonic Substrates. The synthesis of the Au NCA substrate is accomplished via the integration of reactive ion etching (RIE) and magnetic sputtering deposition technology, which is further elaborated in Figure 1.

As per the literature, the 120 nm PS colloidal spheres suspension and ethanol were first ultrasonically dispersed in a ratio of 1:2 (250 and 500 nm PS colloidal spheres in the ratio of 1:1.5 and 1:1, respectively), and then a PS colloidal spheres close-packed single layer was developed on a 3 cm × 3 cm Si (100) wafer via air−liquid interface self-assembly method, as illustrated in Figure 1a.[36,37] The sample was dried at 60 °C for 20 min, and the Si wafer coated with the PS colloidal spheres monolayer template was etched in a reactive ion etching (RIE) instrument, utilizing SF_6, Ar, and CHF_3 plasma (with a flow rate of 20, 10, and 10 sccm/min, respectively, under an etching power of 150 W and a cavity pressure of 2.0 Pa). After etching for 30 s, a highly ordered Si nanocone array (Si NCA) was fabricated, with a small residual PS colloidal sphere remaining on the top of the cones, as shown in Figure 1b. The etched samples were then rinsed with ethanol and annealed at 600 °C for 2 h in a muffle furnace to eliminate the residual PS spheres, leading to the formation of the Si NCA (Figure 1c). Finally, an Au layer was deposited onto the Si NCA through the Au-sputtering process with a deposition rate equivalent to 12.5 nm/min and 30 mA deposition current for a specific time in the Q150R plus Sputter Coating System, as presented in Figure 1d. The Au layer deposition thickness was regulated by adjusting the sputtering time. The as-prepared Au NCA substrate was then divided meticulously into numerous small fragments measuring approximately 3 mm × 3 mm.

2.4. Raman Spectral Measurements. In this study, the treated serum samples were subjected to dilution with ultrapure water to generate serum solutions with varying dilution ratios (10, 50, 100, 500, 1000, 10 000). Subsequently, 3 μL of serum solution with different dilution levels were added to an Au NCA substrate, and the SERS spectra were directly detected after drying naturally at room temperature, as depicted in Figure 1e. The Raman spectral measurements were performed using a confocal Raman spectrometer (RENISHAW Invia Raman Microscope) with an excitation wavelength of 785 nm. The laser beam had a spot diameter of 1 μm on the SERS substrate. The laser power and integral time for all serum Raman spectral measurements were 1 mW and 1 s, respectively. The Raman spectra of serum samples were measured in the wave number range of 400−1800 cm^{-1}, and all obtained Raman spectra were given after baseline correction.

3. RESULTS AND DISCUSSION

3.1. Morphology and Structure. The detection activity and signal reproducibility of substrates are prerequisites for evaluating SERS performances. Noble-metal ordered arrays, due to their excellent signal reproducibility and intense localized plasmonic fields, are widely regarded as outstanding plasmonic substrates.[36] This is attributed to the fact that their tailored microstructure is designed with unit-building blocks and periodic arrangements, which can significantly enhance the localized electromagnetic field by adjusting the structural parameters and composition.[10] In this study, we fabricated uniform and ordered Au NCA plasmonic substrates via reactive ion etching on Si substrates, using PS monolayer as the sacrificial template, followed by surface sputtering deposition.

First, an order-arranged PS colloidal sphere monolayer was fabricated on a Si wafer (3 cm × 3 cm) through air−liquid

https://doi.org/10.1021/acsomega.3c04910
ACS Omega 2023, 8, 29836−29846

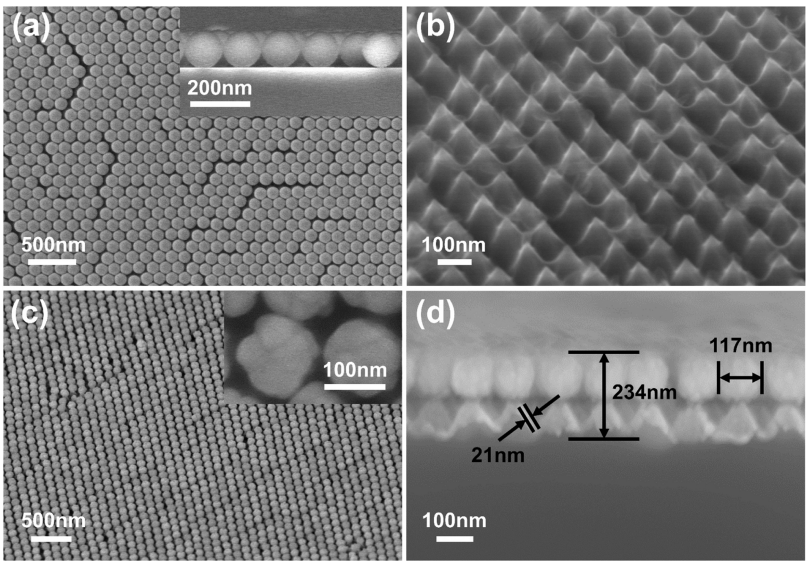

Figure 2. Typical FE-SEM observations during fabrication of Au NCA plasmonic substrate. (a) Self-assembled PS monolayer on Si substrate; inset: cross-sectional view of the monolayer. (b) Si NCA obtained after annealing. (c, d) Oblique and cross-sectional views of the prepared Au NCA, respectively. The inset in (c) shows a magnified view of a single Au NCA.

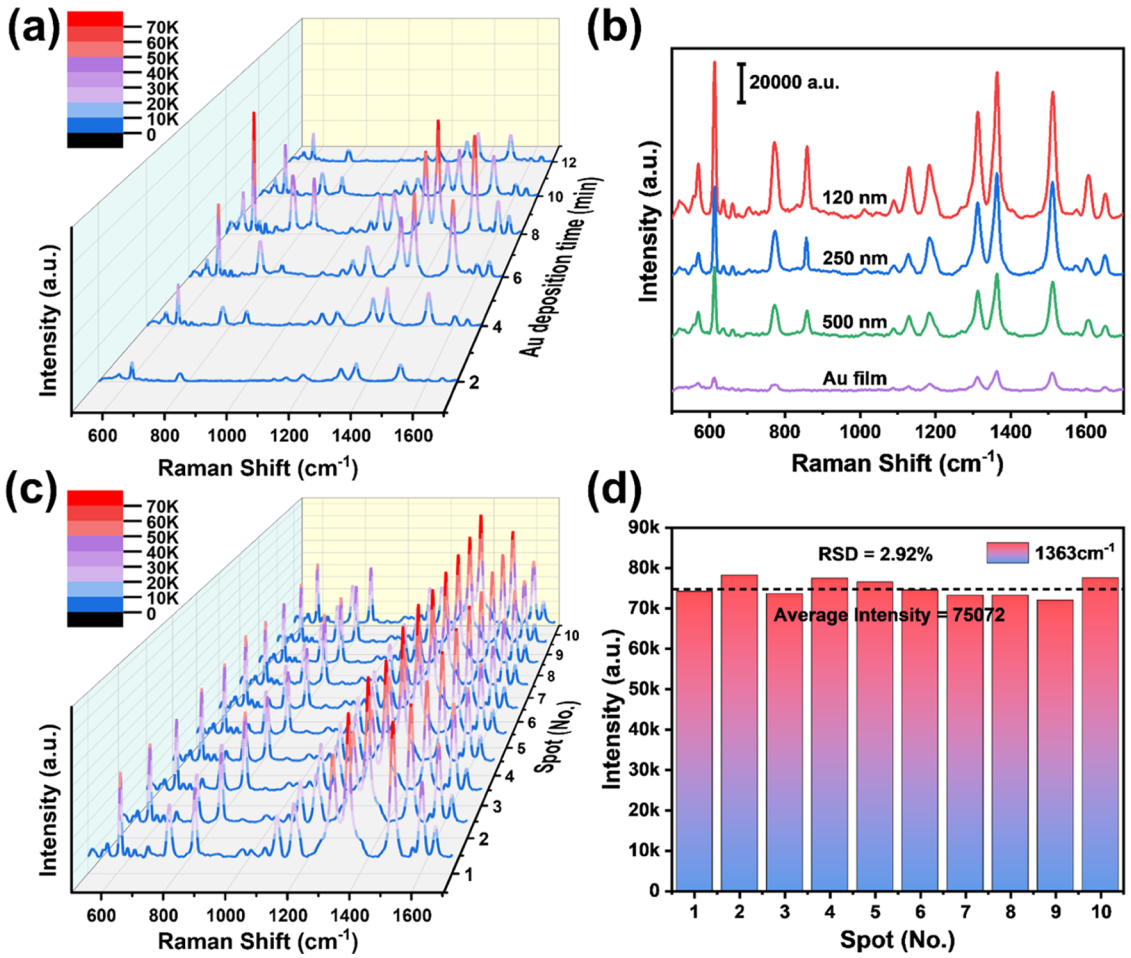

Figure 3. Raman spectra measured on different SERS substrates and the study of spectral repeatability. (a) Raman spectra of the R6G-soaked Au NCA plasmonic substrates with different Au deposition times (deposition rate of 12.5 nm/min). (b) Raman spectral measurements for the R6G-soaked Au NCAs with the periods of 120 nm (red curve), 250 nm (blue curve), and 500 nm (green curve), and the R6G-soaked Au nanoparticle film (purple curve). (c) Raman spectra of R6G collected from 10 randomly selected points on a 1 cm × 1 cm Au NCA plasmonic substrate. (d) Histogram of the peak intensities at 1363 cm^{-1} [data from (c)]. All substrates were immersed in the 10^{-5} M R6G aqueous solution for 90 min before Raman spectral measurements.

https://doi.org/10.1021/acsomega.3c04910
ACS Omega 2023, 8, 29836−29846

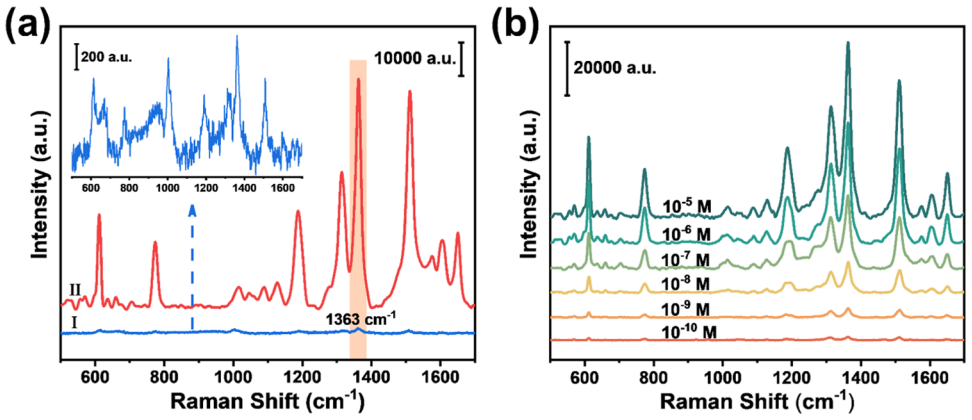

Figure 4. Sensitivity of the Au NCA plasmonic substrate. (a) SERS spectra of 5 μL 10^{-5} M R6G obtained on the Au NCA plasmonic substrate (curve II) and Raman spectra of 10 μL of 0.1 M R6G obtained on a Si wafer (curve I). The inset shows a magnified view of the blue curve. (b) Concentration-dependent SERS spectra obtained by detecting R6G molecules on the Au NCA plasmonic substrate.

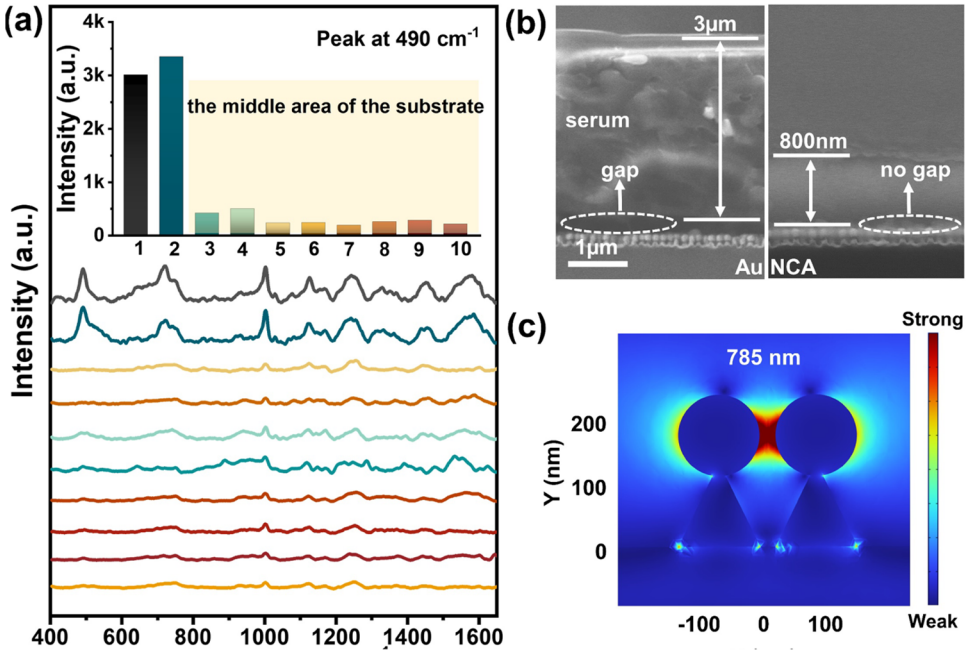

Figure 5. (a) Raman spectra of serum collected from 10 different spots randomly selected from the Au NCA plasmonic substrate after adding 3 μL of serum sample, with a histogram of peak intensity at 490 cm^{-1}. (b) Cross-sectional FE-SEM image of the Au NCA plasmonic substrate after adding 3 μL of serum sample and (c) the simulation diagram of EM enhancement effect around Au NCA under 785 nm wavelength laser excitation.

interface self-assembly. The close-packed hexagonal arrangement of PS spheres with a diameter of 120 nm was observed by field emission scanning electron microscopy (FE-SEM), as shown in Figure 2a. After plasma etching (SF_6, Ar, and CHF_3) and annealing, Si NCAs were formed on the Si wafer surface due to the geometry shape of the PS colloidal sphere template, as shown in Figure 2b. Au NCA plasmonic substrates were obtained after depositing a layer of Au film on the Si NCAs (with a deposition time of 8 min), as shown in Figure 2c. The results show that the array consists of nearly spherical particles measuring approximately 117 nm, composed of multiple 30–50 nm Au nanoparticles (Au NPs) stacked together, resulting in a very rough surface (inset of Figure 2c). There were also abundant nanogaps between the Au NPs, producing exceptional "hotspots" that amplified Raman vibrations of targeted analytes significantly. Observations of the cross section (Figure 2d) indicated that these nearly spherical Au particles were located on top of each Si nanocone, with an approximately 21 nm thick Au film wrapping around the lower part of the Si nanocone.

3.2. Reliable Au NCA Plasmonic Substrates. We choose R6G as a probe to evaluate the SERS performance of Au NCA plasmonic substrates. The substrates with different Au deposition times were soaked in 10^{-5} M R6G aqueous solution for 90 min and then taken out for Raman measurement. The observed Raman spectra of R6G molecules showed strong signals on substrates with a Au deposition time ranging from 6 to 8 min, and the best enhancement effect was obtained with an Au deposition time of 8 min, as shown in Figure 3a. Deviating from this range weakened the Raman signals due to the limited density of the "hotspots" on the substrates caused by an increase in distance between Au nanoparticles or their aggregation. The SERS activities of substrates with different periods and Au nanoparticle films

https://doi.org/10.1021/acsomega.3c04910
ACS Omega 2023, 8, 29836−29846

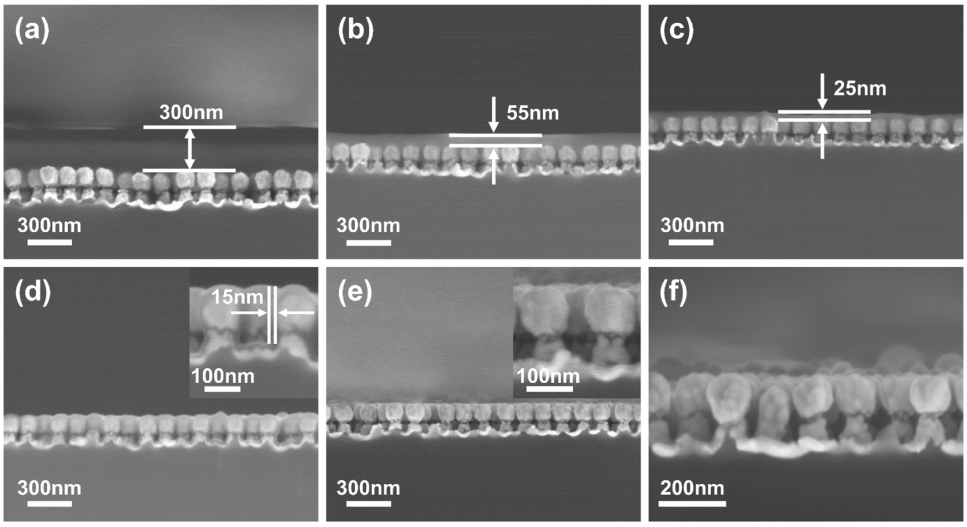

Figure 6. Cross-sectional FE-SEM images of serum droplets diluted at 10 times (a), 50 times (b), 100 times (c), 500 times (d), 1000 times (e), and 10 000 times (f) on the Au NCA substrate. The insets in (d) and (e) are local enlarged images of the corresponding substrates, respectively.

(which were directly deposited on the Si wafer for 8 min) were compared under the same testing conditions, as shown in Figure 3b. The results indicate that the Raman signal of R6G obtained with the substrate having a period of 120 nm was significantly higher than that of substrates with larger periods of 250, 500 nm, and Au nanoparticle films. This is because a smaller arrangement period of Au particles in the array provides a higher density of ″hotspots″, including small nanogaps and rough surfaces. As a result, we choose Au NCA with a period of 120 nm and an Au deposition time of 8 min as the preferred substrate for further research.

The Au NCA plasmonic substrates demonstrate remarkable structural uniformity at the microscale due to the high-quality PS colloidal sphere monolayer template and small-sized PS spheres measuring only 120 nm, which are considerably smaller than a micron. This characteristic leads to a high level of reproducibility when conducting Raman measurements. In order to assess the detection repeatability of the prepared Au NCA plasmonic substrates, we randomly selected 10 points from the 1 cm × 1 cm substrate, and collected 10 SERS spectra of 10^{-5} M R6G molecules, as displayed in Figure 3c. The relative standard deviation (RSD) of the characteristic peak intensities was small, typically less than 2.92% for the peak at 1363 cm^{-1}, as portrayed in Figure 3d, indicating that this method based on template etching and deposition can guarantee excellent signal reproducibility of the substrate.

To quantitatively evaluate the SERS enhancement effect of the selected Au NCA plasmonic substrate, 5 μL of 10^{-5} M and 10 μL of 0.1 M R6G aqueous solutions were dropped on the Au NCA plasmonic substrate and a Si wafer with an area of 9 mm^2 for SERS detection, respectively (Figure 4a). For the vibration at 1363 cm^{-1} of R6G, the enhancement factor (EF) estimated was up to 1.9×10^6, indicating the extremely strong SERS enhancement of the Au NCA plasmonic substrate. In addition, we also explored the detection limit of the Au NCA plasmonic substrate, as shown in Figure 4b. It can be found that the lower limit of the concentration of the substrate to detect R6G can reach 10^{-10} M, further demonstrating the high sensitivity of the substrate.

3.3. SERS-Based Detection of Serum Samples. As is well known, signal reproducibility is excellent in solid-state substrates that possess intense, localized plasmonic fields. The uniformly controllable Au NCA plasmonic substrate prepared above has a high uniformity of structure and similar SERS hotspot density, which is conducive to obtaining a stable, consistent, and strong SERS spectra of serum.

3.3.1. Instability of Direct Serum SERS Analysis. 3 μL of serum samples was dropped on the Au NCA plasmonic substrate for tentative SERS detection. As shown in Figure 5a, we randomly selected 10 points on the substrate for spectra acquisition. We noticed considerable instability in the SERS spectra in different areas of the substrate, with only weak serum SERS spectra detected in most of the central region of the substrate, while strong and complete SERS spectra were obtained in the edge region of the substrate. The predictable signal uniformity of the Au NCA plasmonic substrate suggests that the instability could arise from the serum on the Au NCA plasmonic substrate. For further investigation, we conducted scanning electron microscopy to examine a cross section of the serum sample, as depicted in Figure 5b. We identified that the central region of the substrate had an excessively thick serum layer of approximately 3 μm, which did not tightly cover the Au NCA and left a gap between the serum layer and Au NCA. Comparatively, the serum in the edge region was only a few hundred nanometers thick and closely covered the Au NCA. Based on the foregoing, we suggest that the instability of the serum SERS spectra could arise from the high viscosity and excessive thickness of the serum sample.

To investigate the effect of serum thickness on the SERS spectra, we simulated the electromagnetic enhancement of the as-prepared Au NCA, as depicted in Figure 5c. The distribution of the local electromagnetic field over the surface of the Au NCA plasmonic substrate revealed that a uniform dissemination of target molecules, filling gaps and covering the Au NCA surface evenly, is imperative to obtaining a stable SERS spectrum. Strong and stable SERS enhancement by Au NCA is possible only when serum molecules are homogeneously dispersed in the gaps and on the surface. When serum thickness exceeds the electromagnetic enhancement area of the Au NCA, it is not possible to obtain a consistent and standard SERS spectrum. The findings suggest that there exist some flaws in measuring serum SERS spectra on an Au NCA

https://doi.org/10.1021/acsomega.3c04910
ACS Omega 2023, 8, 29836−29846

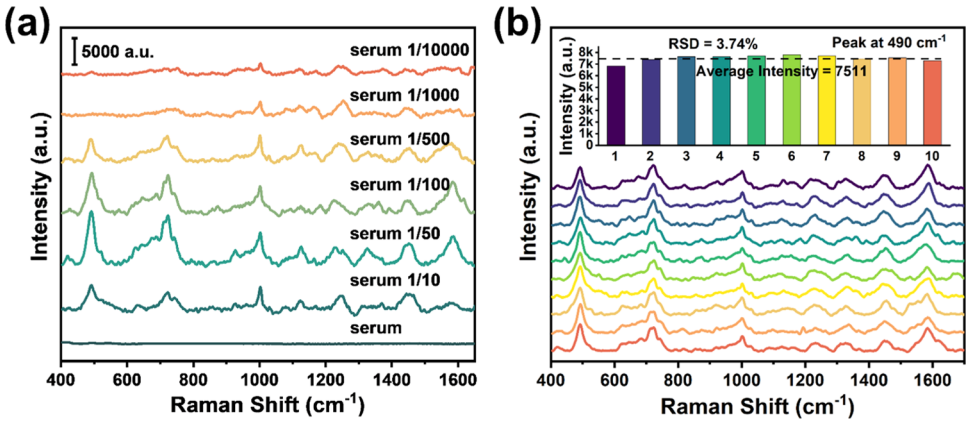

Figure 7. (a) SERS spectra of serum samples with different dilutions (10, 50, 100, 500, 1000, 10 000) obtained under 785 nm laser wavelength excitation. (b) SERS spectra collected from 10 randomly selected different spots on the substrate with 3 μL of serum diluted 50 times, after denoising and smoothing. The inset is the histogram of the peak intensity at 490 cm^{-1}.

plasmonic substrate. The stability and integrity of serum SERS spectra depend critically on serum thickness and viscosity. To obtain vigorous and reliable serum SERS spectra, it is essential to dilute the serum.

3.3.2. Concentration Optimization for High-Quality Serum SERS Spectra. To achieve uniform and effective dispersion of serum molecules on the Au NCA plasmonic substrate, a progressive dilution method was employed, followed by dropwise application of the serum to the substrate. Figure 6a–f shows the FE-SEM images of serum samples acquired at different dilution factors (10, 50, 100, 500, 1000, 10 000). As observed, the diluted serum samples attain a thinner, more even coverage of the Au NCA plasmonic substrate compared to the undiluted serum, ameliorating thick serum layers and high serum viscosity issues. Moreover, through the comparison, it is evident that with the gradual dilution of serum samples, the viscosity of serum decreases continuously, greatly improving its dispersibility and reducing the thickness of the liquid film formed by serum samples on the Au NCA substrate. When the serum dilution factor is 50–500 times, the thickness of the serum layer on the Au NCA substrate is only 15–55 nm, which is conducive to the collection of serum SERS spectra. However, when the serum dilution factors exceed 1000 times, a paucity of serum molecules on the Au NCA plasmonic substrate discourages the effective acquisition of SERS spectra.

Figure 7a exhibits the corresponding SERS spectra of serum samples at different dilution factors under 785 nm laser excitation. As evidenced by the figure, the SERS peaks of the serum are the most comprehensive and possess the highest intensity when the serum is diluted by 50 times, indicating that the optimal sample dilution factor is 50 times. The distinct assignment of characteristic peaks of SERS spectra of normal human serum based on biomolecules is shown in Table 1.[38−42] Figure 7b presents the spectrogram after noise reduction and smoothing collected from 10 different spots randomly selected on the substrate with 3 μL of serum diluted 50 times. It can be clearly seen that the SERS spectra acquired are stable, reproducible, and standardized under 785 nm laser excitation when the serum is diluted 50 times, with a relative standard deviation (RSD) of less than 3.74% for the peak intensity at 490 cm^{-1}. These results demonstrate the importance of optimizing serum concentration for obtaining stable, reproducible, and standardized SERS serum spectra.

Table 1. Distribution of SERS Peaks in Normal Human Serum[43−45]

Raman shift (cm^{-1})	vibrational mode	assignment
427	\	cholesterol and cholesterol ester
490	C deformation to vibration	isoleucine
554	S–S stretching vibration	tryptophan
625	δ (C–S)	tyrosine
726	C–H bending vibration, C–S anti conformation	nucleic acid
857	C–H indole ring vibration	phosphatidic acid
921	\	glycogen and lactic acid
968	C–N deformation vibration	nucleic acid
1006	ring breathing vibration	tryptophan, histidine, and phenylalanine
1089	phospholipid C–C stretching vibration	nucleic acid and lipid
1129	C–C stretching vibration	protein, phospholipid, and saccharides
1218	ring breathing vibration	phenylalanine
1312	ring symmetric stretching methylene CH_2 bending vibration	tryptophan and lipid
1439	CH_2 bending or scissoring	protein and phospholipid
1578	\	tyrosine, tryptophan, and phenylalanine

3.3.3. SERS Detection of Serum for Disease Diagnosis. To verify the accuracy of the optimized serum detection protocol and its practical utility in disease diagnosis, we compared and analyzed the difference in average SERS spectra of normal serum samples and gastric cancer serum samples, following noise reduction and smoothing. As shown in Figure 8a, the two curves have certain similarities in shape, but the SERS intensities of many peaks vary significantly. Noticeable differences emerge between the normal serum and gastric cancer serum at multiple peak positions such as 726, 1006, 1129, 1218, 1312, 1439, and 1578 cm^{-1}. A synthesis of these results and Table 1 demonstrates higher levels of nucleic acids and lower levels of certain proteins in the serum of gastric cancer patients, which indicates the process of carcinogenesis. As gastric cancer cells undergo metabolic and proliferative activities, large quantities of proteins are shed, causing a relatively higher concentration of nucleic acids in the serum.

https://doi.org/10.1021/acsomega.3c04910
ACS Omega 2023, 8, 29836−29846

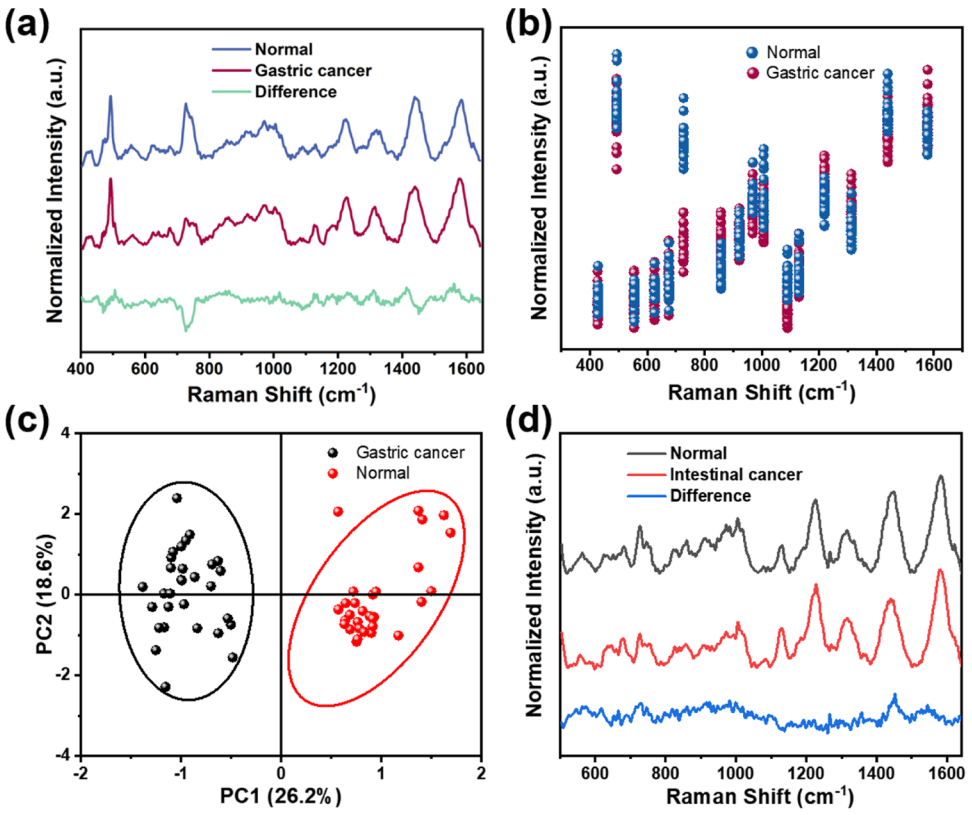

Figure 8. (a) Differences in serum SERS spectra between normal individuals and gastric cancer patients. (b) Scatter diagram of different bands of serum SERS spectra between the normal group (30 healthy volunteers) and the gastric cancer group (30 gastric cancer patients). (c) Two-dimensional score diagram of the normal group and the gastric cancer group. (d) SERS detection of intestinal cancer patients' serum. Differences in SERS spectra between normal individuals and intestinal cancer patients' serum.

These outcomes align with prior scientific research on gastric cancer.[43−45] The scatter diagram of the corresponding difference bands is shown in Figure 8b, which can well reflect the difference bands of the serum SERS spectra of the normal group (30 healthy volunteers) and the gastric cancer group (30 gastric cancer patients). To evaluate the feasibility of utilizing serum SERS spectra acquired via an optimized serum SERS detection scheme based on Au NCA solid substrate in the realm of disease diagnosis, we conducted a statistical analysis on the SERS spectra data of serum from the normal group and the gastric cancer group, utilizing the principal component analysis (PCA) method. A two-dimensional score diagram of the SERS spectra of serum from the normal and gastric cancer groups is depicted in Figure 8c. It is evident that the SERS spectra of serum from both groups exhibited distinct clustering, with discernible boundaries between them. This demonstrates that the acquired serum SERS spectra can effectively differentiate between the normal and gastric cancer groups using the PCA method. At the same time, we also applied this approach to the diagnosis of other diseases, such as intestinal cancer. As shown in Figure 8d, it can effectively differentiate the serum spectra of normal individuals and intestinal cancer patients. The experiment further proves that the uniform and controllable Au NCA plasmonic substrate and the optimized serum SERS detection scheme prepared in this study have broad practical application value in serum detection, and are expected to be used in the diagnosis of actual diseases. Therefore, this research provides a new strategy and method for the practical application of SERS-based biosensors, expected to assist in the advancement of clinical medicine, as well as diagnosis and treatment.

4. CONCLUSIONS

In the present work, a high-activity Au nanocone array (Au NCA) plasmonic substrate with microstructures was successfully prepared using the reactive ion etching (RIE) assisted by PS colloidal sphere template and magnetron sputtering deposition technology. The Au NCA plasmonic substrate was used as the active substrate for SERS, and the instability of SERS spectra of normal human serum was analyzed. The optimal dilution conditions of serum were optimized, and serum thickness and viscosity were evaluated to establish a standard detection method for highly stable and repeatable serum SERS spectra based on the Au NCA plasmonic substrate. In addition, the optimized serum detection method was applied to diagnose gastric cancer. The average difference spectra of normal individuals and gastric cancer patients were analyzed after noise reduction and smoothing. This helped extract significant differential bands between the two groups, further confirming the reliability of the optimized serum detection method. The serum SERS detection scheme based on the Au NCA plasmonic substrate proposed in this experiment rationalizes the instability of the serum spectrum, providing a solid foundation for establishing a standard serum SERS detection method and necessary prerequisites for conducting reliable SERS-based diagnostic technologies.

https://doi.org/10.1021/acsomega.3c04910
ACS Omega 2023, 8, 29836−29846

AUTHOR INFORMATION

Corresponding Authors

Qian Zhao − *Key Lab of Materials Physics, Anhui Key Lab of Nanomaterials and Nanotechnology, Institute of Solid State Physics, HFIPS, Chinese Academy of Sciences, Hefei 230031, P. R. China*; Email: zhaoqian@issp.ac.cn

Yu Ouyang − *Department of Clinical Laboratory, The Affiliated Taizhou Second People's Hospital of Yangzhou University, Taizhou 225300, P. R. China*; Email: 15751177628@yzu.edu.cn

Hongwen Zhang − *Key Lab of Materials Physics, Anhui Key Lab of Nanomaterials and Nanotechnology, Institute of Solid State Physics, HFIPS, Chinese Academy of Sciences, Hefei 230031, P. R. China; Lu'an Branch, Anhui Institute of Innovation for Industrial Technology, Lu'an 237100, P. R. China*; orcid.org/0000-0002-1358-7336; Email: hwzhang@issp.ac.cn

Authors

Yanyan Lu − *Key Lab of Materials Physics, Anhui Key Lab of Nanomaterials and Nanotechnology, Institute of Solid State Physics, HFIPS, Chinese Academy of Sciences, Hefei 230031, P. R. China; University of Science and Technology of China, Hefei 230026, P. R. China*

Biao Lei − *Key Lab of Materials Physics, Anhui Key Lab of Nanomaterials and Nanotechnology, Institute of Solid State Physics, HFIPS, Chinese Academy of Sciences, Hefei 230031, P. R. China; University of Science and Technology of China, Hefei 230026, P. R. China*

Xiaowei Yang − *Key Lab of Materials Physics, Anhui Key Lab of Nanomaterials and Nanotechnology, Institute of Solid State Physics, HFIPS, Chinese Academy of Sciences, Hefei 230031, P. R. China; University of Science and Technology of China, Hefei 230026, P. R. China*

Yi Wei − *Key Lab of Materials Physics, Anhui Key Lab of Nanomaterials and Nanotechnology, Institute of Solid State Physics, HFIPS, Chinese Academy of Sciences, Hefei 230031, P. R. China*

Tingting Xiao − *Key Lab of Materials Physics, Anhui Key Lab of Nanomaterials and Nanotechnology, Institute of Solid State Physics, HFIPS, Chinese Academy of Sciences, Hefei 230031, P. R. China*

Shuyi Zhu − *Key Lab of Materials Physics, Anhui Key Lab of Nanomaterials and Nanotechnology, Institute of Solid State Physics, HFIPS, Chinese Academy of Sciences, Hefei 230031, P. R. China; University of Science and Technology of China, Hefei 230026, P. R. China*

Weiping Cai − *Key Lab of Materials Physics, Anhui Key Lab of Nanomaterials and Nanotechnology, Institute of Solid State Physics, HFIPS, Chinese Academy of Sciences, Hefei 230031, P. R. China; University of Science and Technology of China, Hefei 230026, P. R. China*; orcid.org/0000-0002-4515-6098

Complete contact information is available at: https://pubs.acs.org/10.1021/acsomega.3c04910

Author Contributions

Y.Y.L.: Investigation, validation, data curation, writing—original draft. Q.Z.: Investigation, visualization, writing—editing. B.L.: Investigation, validation, data curation. X.W.Y., T.T.X.: Data analysis. Y.O.: Investigation, methodology. H.W.Z.: Methodology, formal analysis, funding acquisition, writing—review and editing. Y.W., S.Y.Z.: Visualization, methodology, formal analysis. W.P.C.: Project administration, funding acquisition.

Funding

This work was financially supported by National Natural Science Foundation of China (grant nos. 52271242, 51971209, and 52201167), Science and Technology Bureau of Jiangyan District (grant no. 2020307), and Taizhou "Fengcheng Talent Plan" Young Science and Technology Talent Lifting Project.

Notes

The authors declare no competing financial interest.

The studies involving human participants were reviewed and approved by the Ethics Committee of Hefei Institutes of Physical Science (HFIPS), Chinese Academy of Sciences.

REFERENCES

(1) Langer, J.; de Aberasturi, D. J.; Aizpurua, J.; Alvarez-Puebla, R. A.; Auguie, B.; Baumberg, J. J.; Bazan, G. C.; Bell, S. E. J.; Boisen, A.; Brolo, A. G.; Choo, J.; Cialla-May, D.; Deckert, V.; Fabris, L.; Faulds, K.; de Abajo, F. J. G.; Goodacre, R.; Graham, D.; Haes, A. J.; Haynes, C. L.; Huck, C.; Itoh, T.; Ka, M.; Kneipp, J.; Kotov, N. A.; Kuang, H.; Le Ru, E. C.; Lee, H. K.; Li, J. F.; Ling, X. Y.; Maier, S. A.; Mayerhofer, T.; Moskovits, M.; Murakoshi, K.; Nam, J. M.; Nie, S.; Ozaki, Y.; Pastoriza-Santos, I.; Perez-Juste, J.; Popp, J.; Pucci, A.; Reich, S.; Ren, B.; Schatz, G. C.; Shegai, T.; Schlucker, S.; Tay, L. L.; Thomas, K. G.; Tian, Z. Q.; Van Duyne, R. P.; Vo-Dinh, T.; Wang, Y.; Willets, K. A.; Xu, C.; Xu, H.; Xu, Y.; Yamamoto, Y. S.; Zhao, B.; Liz-Marzan, L. M. Present and Future of Surface-Enhanced Raman Scattering. *ACS Nano* **2020**, *14*, 28−117.

(2) Han, Q. Y.; Zhang, C. Y.; Gao, W.; Han, Z. H.; Liu, T. Z.; Li, C. X.; Wang, Z. J.; He, E. J.; Zheng, H. R. Ag-Au Alloy Nanoparticles: Synthesis and in Situ Monitoring SERS of Plasmonic Catalysis. *Sens. Actuators, B* **2016**, *231*, 609−614.

(3) Zhang, Z. L.; Xu, P.; Yang, X. Z.; Liang, W. J.; Sun, M. T. Surface Plasmon-Driven Photocatalysis in Ambient, Aqueous and High-Vacuum Monitored by SERS and TERS. *J. Photochem. Photobiol., C* **2016**, *27*, 100−112.

(4) Koh, C. S. L.; Lee, H. K.; Phan-Quang, G. C.; Han, X. M.; Lee, M. R.; Yang, Z.; Ling, X. Y. SERS- and Electrochemically Active 3D Plasmonic Liquid Marbles for Molecular-Level Spectroelectrochemical Investigation of Microliter Reactions. *Angew. Chem., Int. Ed.* **2017**, *56*, 8813−8817.

(5) Zaleski, S.; Wilson, A. J.; Mattei, M.; Chen, X.; Goubert, G.; Cardinal, M. F.; Willets, K. A.; Van Duyne, R. P. Investigating Nanoscale Electrochemistry with Surface- and Tip-Enhanced Raman Spectroscopy. *Acc. Chem. Res.* **2016**, *49*, 2023−2030.

(6) Li, Q. Q.; Huo, H. Q.; Wu, Y.; Chen, L. L.; Su, L. C.; Zhang, X.; Song, J. B.; Yang, H. H. Design and Synthesis of SERS Materials for In Vivo Molecular Imaging and Biosensing. *Adv. Sci.* **2023**, *10*, No. 2202051.

(7) Zhang, K.; Wang, Y. N.; Wu, M. L.; Liu, Y. J.; Shi, D. Y.; Liu, B. H. On-Demand Quantitative SERS Bioassays Facilitated by Surface-Tethered Ratiometric Probes. *Chem. Sci.* **2018**, *9*, 8089−8093.

(8) Huang, Z. C.; Zhang, A. M.; Zhang, Q.; Cui, D. X. Nanomaterial-Based SERS Sensing Technology for Biomedical Application. *J. Mater. Chem. B* **2019**, *7*, 3755−3774.

(9) Wu, L.; Teixeira, A.; Garrido-Maestu, A.; Muinelo-Romay, L.; Lima, L.; Santos, L. L.; Prado, M.; Dieguez, L. Profiling DNA Mutation Patterns by SERS Fingerprinting for Supervised Cancer Classification. *Biosens. Bioelectron.* **2020**, *165*, No. 112392.

(10) Xu, W. S.; Bao, H. M.; Zhang, H. W.; Fu, H.; Zhao, Q.; Li, Y.; Cai, W. P. Ultrasensitive Surface-Enhanced Raman Spectroscopy Detection of Gaseous Sulfur-Mustard Simulant Based on Thin Oxide-Coated Gold Nanocone Arrays. *J. Hazard. Mater.* **2021**, *420*, No. 126668.

(11) Zhao, Z. P.; Bao, H. M.; Zhao, Q.; Fu, H.; Zhou, L.; Zhang, H. W.; Li, Y.; Cai, W. P. Efficient SERS Response of Porous-ZnO-

https://doi.org/10.1021/acsomega.3c04910
ACS Omega 2023, 8, 29836−29846

Covered Gold Nanoarray Chips to Trace Benzene-Volatile Organic Compounds. *ACS Appl. Mater. Interfaces* **2022**, *14*, 47999−48010.
(12) Kim, W.; Lee, S. H.; Kim, J. H.; Ahn, Y. J.; Kim, Y. H.; Yu, J. S.; Choi, S. Paper-Based Surface-Enhanced Raman Spectroscopy for Diagnosing Prenatal Diseases in Women. *ACS Nano* **2018**, *12*, 7100−7108.
(13) Girish, C. M.; Iyer, S.; Thankappan, K.; Rani, V. V. D.; Gowd, G. S.; Menon, D.; Nair, S.; Koyakutty, M. Rapid Detection of Oral Cancer Using Ag-TiO_2 Nanostructured Surface-Enhanced Raman Spectroscopic Substrates. *J. Mater. Chem. B* **2014**, *2*, 989−998.
(14) Kang, T.; Kim, H.; Lee, J. M.; Lee, H.; Choi, Y. S.; Kang, G.; Seo, M. K.; Chung, B. H.; Jung, Y.; Kim, B. Ultra-Specific Zeptomole MicroRNA Detection by Plasmonic Nanowire Interstice Sensor with Bi-Temperature Hybridization. *Small* **2014**, *10*, 4200−4206.
(15) He, X. Y.; Ge, C.; Zheng, X. Q.; Tang, B.; Chen, L.; Li, S. B.; Wang, L.; Zhang, L. Q.; Xu, Y. Rapid Identification of Alpha-Fetoprotein in Serum by a Microfluidic SERS Chip Integrated with Ag/Au Nanocomposites. *Sens. Actuators, B* **2020**, *317*, No. 128196.
(16) Neugebauer, U.; Rosch, P.; Popp, J. Raman Spectroscopy towards Clinical Application: Drug Monitoring and Pathogen Identification. *Int. J. Antimicrob. Agents* **2015**, *46*, S35−S39.
(17) Shi, W.; Paproski, R. J.; Moore, R.; Zemp, R. Detection of Circulating Tumor Cells Using Targeted Surface-Enhanced Raman Scattering Nanoparticles and Magnetic Enrichment. *J. Biomed. Opt.* **2014**, *19*, No. 056014.
(18) Tabakman, S. M.; Chen, Z.; Casalongue, H. S.; Wang, H. L.; Dai, H. J. A New Approach to Solution-Phase Gold Seeding for SERS Substrates. *Small* **2011**, *7*, 499−505.
(19) Brown, G. C.; Veronelli, J. A.; Maassab, H. F.; Francis, T. J. Rubella Antibodies in Human Serum-Detection by Indirect Fluorescent-Antibody Technique. *Science* **1964**, *145*, 943−945.
(20) Ibrahim, H. A. Relationship Between Helicobacter pylori Infection, Serum Vitamin D3 Level and Spontaneous Abortion. *Int. J. Gen. Med.* **2020**, *13*, 469−476.
(21) Zajac, V.; Altaner, C. Diagnosis of Bovine Leukosis Virus-Infection by Solid-Phase Radioimmunoassay for Virus-Antibody. *Neoplasma* **1981**, *28*, 661−668.
(22) Pan, X.; Li, L. H.; Lin, H. D.; Tan, J. Y.; Wang, H. T.; Liao, M. L.; Chen, C. J.; Shan, B. B.; Chen, Y. F.; Li, M. A Graphene Oxide-Gold Nanostar Hybrid Based-Paper Biosensor for Label-Free SERS Detection of Serum Bilirubin for Diagnosis of Jaundice. *Biosens. Bioelectron.* **2019**, *145*, No. 111713.
(23) Zhao, L. L.; Blackburn, J.; Brosseau, C. L. Quantitative Detection of Uric Acid by Electrochemical-Surface Enhanced Raman Spectroscopy Using a Multi layered Au/Ag Substrate. *Anal. Chem.* **2015**, *87*, 441−447.
(24) Muhammad, M.; Shao, C. S.; Huang, Q. Aptamer-Functionalized Au Nanoparticles Array as the Affective SERS Biosensor for Label-Free Detection of Interleukin-6 In Serum. *Sens. Actuators, B* **2021**, *334*, 129607.
(25) Wang, J.; Lin, D.; Lin, J. Q.; Yu, Y.; Huang, Z. F.; Chen, Y. P.; Lin, J. Y.; Feng, S. Y.; Li, B. H.; Liu, N. R.; Chen, R. Label-Free Detection of Serum Proteins Using Surface-Enhanced Raman Spectroscopy for Colorectal Cancer Screening. *J. Biomed. Opt.* **2014**, *19*, No. 087003.
(26) Chen, M.; Luo, W.; Zhang, Z. M.; Wang, R. H.; Zhu, Y. Q.; Yang, H.; Chen, X. Q. Synthesis of Multi-Au-Nanoparticle-Embedded Mesoporous Silica Microspheres as Self-Filtering and Reusable Substrates for SERS Detection. *ACS Appl. Mater. Interfaces* **2017**, *9*, 42156−42166.
(27) Dai, X.; Lu, L. W.; Zhang, X. H.; Song, Z. L.; Song, W. J.; Chao, Q. Q.; Li, Q.; Wang, W.; Chen, J. F.; Fan, G. C.; Luo, X. L. MnO_2 Shell-Isolated SERS Nanoprobe For the Quantitative Detection of ALP Activity in Trace Serum: Relying on the Enzyme-Triggered Etching of MnO_2 Shell to Regulate the Signal. *Sens. Actuators, B* **2021**, *334*, No. 129605.
(28) Wang, X. M.; Ma, L.; Sun, S. J.; Liu, T. W.; Zhou, H.; Liu, X. H.; Guan, M. Rapid, Highly Sensitive and Quantitative Detection of Interleukin 6 Based on SERS Magnetic Immunoassay. *Anal. Methods* **2021**, *13*, 1823−1831.
(29) Zhang, H.; Ma, X. Y.; Liu, Y.; Duan, N.; Wu, S. J.; Wang, Z. P.; Xu, B. C. Gold Nanoparticles Enhanced SERS Aptasensor for the Simultaneous Detection of Salmonella Typhimurium and Staphylococcus Aureus. *Biosens. Bioelectron.* **2015**, *74*, 872−877.
(30) Stefancu, A.; Badarinza, M.; Moisoiu, V.; Iancu, S. D.; Serban, O.; Leopold, N.; Fodor, D. SERS-Based Liquid Biopsy of Saliva and Serum From Patients with Sjogren's Syndrome. *Anal. Bioanal. Chem.* **2019**, *411*, 5877−5883.
(31) Szekeres, G. P.; Kneipp, J. Different Binding Sites of Serum Albumins in the Protein Corona of Gold Nanoparticles. *Analyst* **2018**, *143*, 6061−6068.
(32) Zhao, Q.; Zhang, H. W.; Fu, H.; Wei, Y.; Cai, W. P. Raman Reporter-Assisted Au Nanorod Arrays SERS Nanoprobe for Ultrasensitive Detection of Mercuric Ion (Hg^{2+}) with Superior Anti-Interference Performances. *J. Hazard. Mater.* **2020**, *398*, No. 122890.
(33) Wei, Y.; Zhu, Y.-y.; Wang, M.-l. Surface-Enhanced Raman Spectroscopy of Gastric Cancer Serum with Gold Nanoparticles/Silicon Nanowire Arrays. *Optik* **2016**, *127*, 7902−7907.
(34) Muhammad, M.; Shao, C. S.; Huang, Q. Label-Free SERS Diagnostics of Radiation-Induced Injury Via Detecting the Biomarker Raman Signal in the Serum and Urine Bio-Samples Based on Au-NPs Array Substrates. *Spectrochim. Acta, Part A* **2019**, *223*, 117282.
(35) Yue, X.; Zheng, X.; Lv, G.; Mo, J.; Yu, X.; Liu, J.; Jia, Z.; Lv, X.; Tang, J. Synthesis of a Low-Cost, Stable, Silicon-Based SERS Substrate for Rapid, Nondestructive Biosensing. *Optik* **2019**, *192*, No. 162959.
(36) Fu, H.; Bao, H. M.; Zhang, H. W.; Zhao, Q.; Zhou, L.; Zhu, S. Y.; Wei, Y.; Li, Y.; Cai, W. P. Quantitative Surface-Enhanced Raman Spectroscopy for Field Detections Based on Structurally Homogeneous Silver-Coated Silicon Nanocone Arrays. *ACS Omega* **2021**, *6*, 18928−18938.
(37) Liu, D. L.; Cai, W. P.; Marin, M.; Yin, Y. D.; Li, Y. Air-Liquid Interfacial Self-Assembly of Two-Dimensional Periodic Nanostructured Arrays. *Chemnanomat* **2019**, *5*, 1338−1360.
(38) Li, J.; Ding, J.; Liu, X. L.; Tang, B.; Bai, X.; Wang, Y.; Li, S. C.; Wang, X. L. Label-Free Serum Detection of Trichinella Spiralis Using Surface-Enhanced Raman Spectroscopy Combined with Multivariate Analysis. *Acta Trop.* **2020**, *203*, No. 105314.
(39) Liang, X. Z.; Miao, X. C.; Xiao, W. J.; Ye, Q.; Wang, S. S.; Lin, J. Q.; Li, C.; Huang, Z. F. Filter-Membrane-Based Ultrafiltration Coupled with Surface-Enhanced Raman Spectroscopy for Potential Differentiation of Benign and Malignant Thyroid Tumors from Blood Plasma. *Int. J. Nanomed.* **2020**, *15*, 2303−2314.
(40) Liu, K. Y.; Jin, S. Z.; Song, Z. B.; Jiang, L. High Accuracy Detection of Malignant Pleural Effusion Based on Label-Free Surface-Enhanced Raman Spectroscopy and Multivariate Statistical Analysis. *Spectrochim. Acta, Part A* **2020**, *226*, No. 117632.
(41) Shao, L. T.; Zhang, A. Y.; Rong, Z.; Wang, C. W.; Jia, X. F.; Zhang, K. H.; Xiao, R.; Wang, S. Q. Fast and Non-Invasive Serum Detection Technology Based on Surface-Enhanced Raman Spectroscopy and Multivariate Statistical Analysis for Liver Disease. *Nanomed. Nanotechnol.* **2018**, *14*, 451−459.
(42) Qiu, S. F.; Xu, Y. J.; Huang, L. L.; Zheng, W.; Huang, C. B.; Huang, S. H.; Lin, J. Y.; Lin, D.; Feng, S. Y.; Chen, R.; Pan, J. J. Non-Invasive Detection of Nasopharyngeal Carcinoma Using Saliva Surface-Enhanced Raman Spectroscopy. *Oncol. Lett.* **2016**, *11*, 884−890.
(43) Feng, S. Y.; Chen, R.; Lin, J. Q.; Pan, J. J.; Wu, Y. A.; Li, Y. Z.; Chen, J. S.; Zeng, H. S. Gastric Cancer Detection Based on Blood Plasma Surface-Enhanced Raman Spectroscopy Excited by Polarized Laser Light. *Biosens. Bioelectron.* **2011**, *26*, 3167−3174.
(44) Liu, Y. W.; Chen, S.; Xue, R.; Zhao, J.; Di, M. J. Mefloquine Effectively Targets Gastric Cancer Cells through Phosphatase-Dependent Inhibition of PI3K/Akt/mTOR Signaling Pathway. *Biochem. Biophys. Res. Commun.* **2016**, *470*, 350−355.
(45) Yamashita, K.; Ushiku, H.; Katada, N.; Hosoda, K.; Moriya, H.; Mieno, H.; Kikuchi, S.; Hoshi, K.; Watanabe, M. Reduced

https://doi.org/10.1021/acsomega.3c04910
ACS Omega 2023, 8, 29836−29846

Preoperative Serum Albumin and Absence of Peritoneal Dissemination May be Predictive Factors for Long-Term Survival with Advanced Gastric Cancer with Positive Cytology Test. *Euro. J. Surg. Oncol.* **2015**, *41*, 1324−1332.

https://doi.org/10.1021/acsomega.3c04910
ACS Omega 2023, 8, 29836−29846